# Terahertz Modulation by Schottky Junction in Metal-Semiconductor-Metal Microcavities

**Goran Isić[1,2,*], Georgios Sinatkas[3], *Student Member, IEEE*, Dimitrios C. Zografopoulos[4], Borislav Vasić[1], Antonio Ferraro[4], *Member, IEEE*, Romeo Beccherelli[4], *Member, IEEE*, Emmanouil E. Kriezis[3], *Senior Member, IEEE*, and Milivoj Belić[2]**

[1]*Graphene Laboratory of Center for Solid State Physics and New Materials, Institute of Physics Belgrade, University of Belgrade, Pregrevica 118, 11080 Belgrade, Serbia*

[2]*Texas A&M University at Qatar, Doha 23874, Qatar*

[3]*School of Electrical and Computer Engineering, Aristotle University of Thessaloniki, Thessaloniki 52124, Greece*

[4]*Consiglio Nazionale delle Ricerche, Istituto per la Microelettronica e Microsistemi, Rome 00133, Italy*

** Tel: (38111) 3713 050, Fax: (38111) 3162 190, e-mail: isicg@ipb.ac.rs*

**ABSTRACT**

We discuss arrays of metal-semiconductor-metal cavities as electrically tunable terahertz metasurfaces. The operation of the considered device is based on reverse biasing the Schottky junction formed between top metal strips and the n-type semiconductor buried beneath. The effective Drude permittivity of the cavity array is tuned by changing the depletion layer thickness via a gate bias applied between the strips and a back metal reflector. Combining Maxwell equations for terahertz waves with a drift-diffusion model for the semiconductor carriers into a multiphysics framework, we show that the proposed modulation concept is promising for a large part of the terahertz spectrum.

**Keywords**: terahertz metasurface, tunable metamaterial, terahertz modulation, Schottky junction.

## 1. INTRODUCTION

The development of fast electro-optic modulators for free-space terahertz waves is one of the important challenges for terahertz technology and further progress in wireless communications. Following the low modulation efficiencies found in initial experiments [1,2], which were ascribed to weak interaction of the terahertz wave with the electron system [3], recent works have mostly employed resonant metasurfaces for increasing the modulation efficiency [4-10]. In addition to semiconductors which seem to be most promising for high-speed modulation [11], graphene [12] and liquid crystal [13-15] modulators have recently been attracting attention. In contrast to existing semiconductor devices employing antenna-like elements for tuning, here [16] we consider the use of a metal-semiconductor-metal resonant cavity array, known for providing a strong light-matter interaction [17,18].

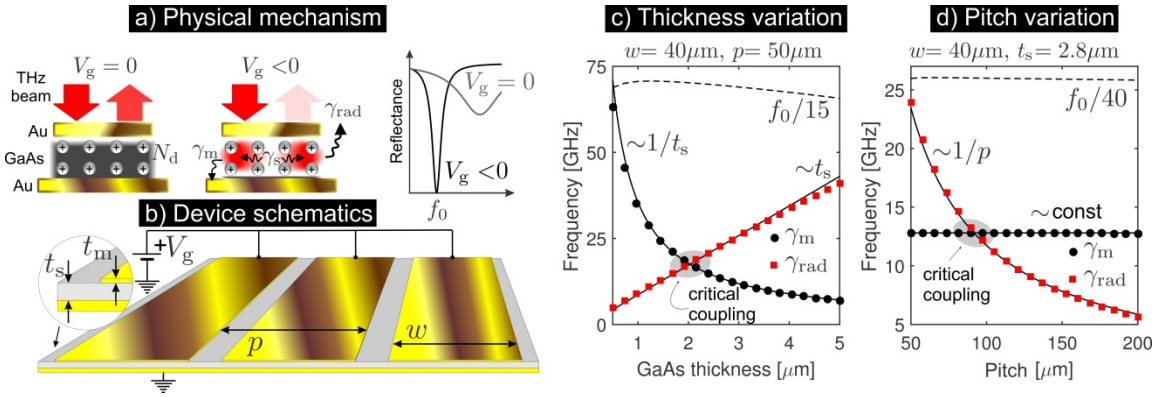


*Figure 1. Schematics of a) cavity-response tuning through carrier depletion and the resulting reflectance modulation, b) real-scale device. c) and d) show the dependence of the TCMT parameters on device geometry.*

## 2. MODULATION PRINCIPLE

The proposed device comprises an array of metal-semiconductor-metal cavities as shown in Figs. 1(a) and 1(b), whereby the semiconductor (gallium arsenide-GaAs) is highly doped and prepared to form a Schottky junction with the top electrode and an ohmic contact with the bottom one. With no bias, the free carriers inhibit the penetration of terahertz fields and strongly dissipate the fields inside the cavity through Joule heating. Upon applying a sufficiently high reverse bias, the depletion layer extends down to the bottom electrode and the cavity is able to support a resonant mode at $f_0$. According to a formalism known as the temporal coupled-mode theory (TCMT) [19,20], in addition to $f_0$, two more parameters are sufficient to fully characterize the resonant optical

response of such a cavity array: the resonant mode non-radiative decay rate $\gamma_0$ and its radiative decay rate $\gamma_{rad}$. $\gamma_0$ is the sum of all absorption mechanisms, including absorption in the metal and Joule losses by the free carriers in GaAs. However, at full cavity depletion, the Joule losses are negligible and $\gamma_0$ becomes equal to the metal absorption rate $\gamma_m$. To achieve optimal performance, in this work we aim at designing the cavities (i.e. choosing their geometrical parameters) so that $\gamma_0 \approx \gamma_{rad}$ which represents the so-called critical coupling regime and results in 100% absorption at $f_0$. Figures 1(c) and 1(d) show how the TCMT parameters depend on the cavity array height and pitch, with further details discussed in [16,21]. The modulation principle is thus based on having 100% absorption at high reverse bias (fully depleted and critically coupled cavity) and a rather inefficient absorption at resonance (typically 10% or less) at zero $V_g$, resulting from the combined detuning of the resonance and its weak coupling with the terahertz wave due to $\gamma_0 >> \gamma_{rad}$.

For purposes of illustration, below we consider the case of a modulator designed to operate at $f_0$=1 THz. The cavity geometrical parameters yielding critical coupling for $f_0$ ranging across the terahertz range can be obtained analogously or even faster by scaling the 1 THz cavity, Fig. 2(a) [20].

The dopant concentration $N_d$ is the final parameter affecting the device operation. Since a higher electron concentration leads to a higher resonance detuning at zero bias, $N_d$ should be as high as possible while still allowing the full depletion of the cavity at the maximal reverse bias $-V_{g,max}$. The latter is estimated via the so-called critical field approximation whereby the junction breakdown is assumed to occur once the electric field at the junction surpasses $4\times10^7$ V/m, which is reasonably accurate for the doping range considered in our work [22]. The gate effect in the considered system is studied using a rigorous solid-state physics framework based on a majority-carrier solution scheme [23,24], while typical electron concentration and electric field profiles for the 1 THz geometry are shown in Figs. 2(b) and 2(c).

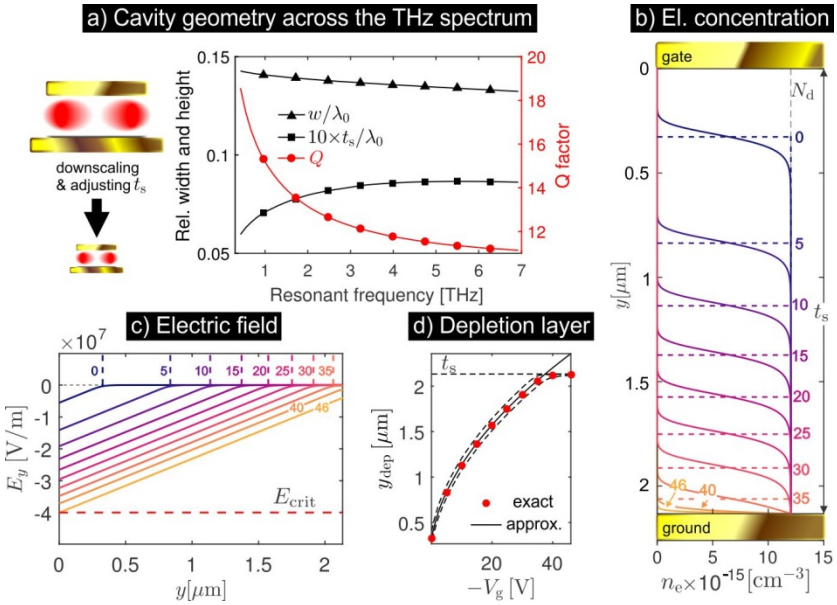


*Figure 2: a) Geometrical parameters of critically coupled cavities drawn across the terahertz spectrum. The behavior of the Schottky junction under reverse bias: b) and c) electron concentration and electric field profile parameterized by $V_g$, d) depletion layer width as a function of $V_g$.*

## 3. PROOF OF CONCEPT

We use a rigorous multiphysics framework incorporating Maxwell equations for terahertz waves and a drift-diffusion model for describing the carrier concentration $n_e(\mathbf{r})$ and mobility $\mu_n$ [25] in GaAs. The two physical models are coupled via the inhomogeneous dielectric permittivity of GaAs [26]

$$\varepsilon_s(\mathbf{r},\omega) = \varepsilon_{opt}\left(1 - \frac{\omega_p^2(\mathbf{r})}{\omega(\omega + i\gamma_c)}\right) \quad (1)$$

where the plasma frequency $\omega_p$ and intraband electron collision rate $\gamma_c$ are given in terms of the GaAs conduction band effective mass $m_c$* and unit charge $q$ as

$$\omega_p^2(\mathbf{r}) = \frac{n_e(\mathbf{r})q^2}{\varepsilon_{opt}\varepsilon_0 m_c^*}, \qquad \gamma_c = \frac{q}{\mu_n m_c^*}. \quad (2)$$

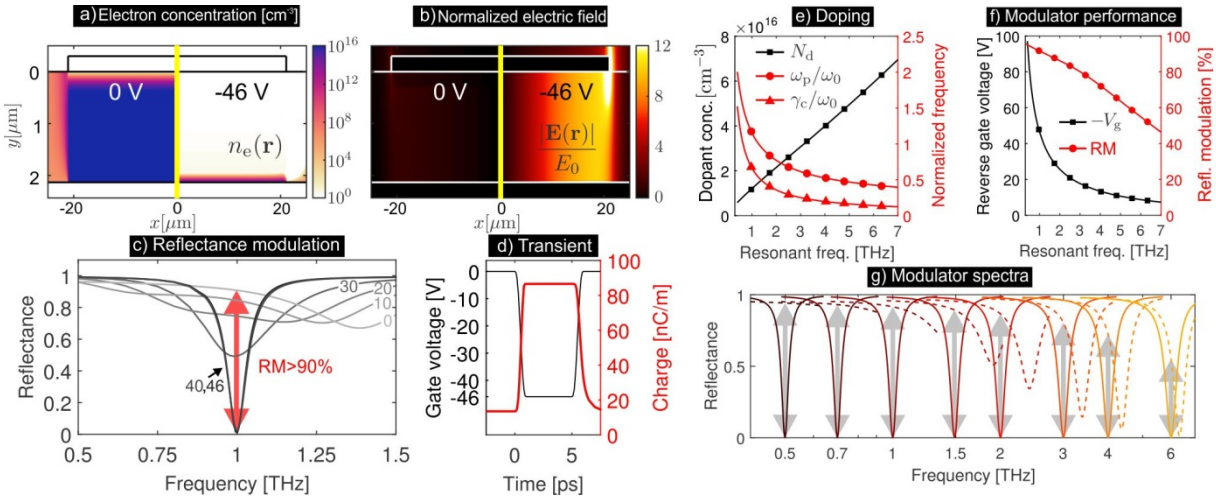


*Figure 3: a)-d) Proof of concept multiphysics simulation results, showing the performance of the device operating at 1 THz. For operating frequencies across the terahertz spectrum, e),f) and g) show the required doping, modulation depth/bias voltage and modulator spectra, respectively.*

The simulation results obtained for the $f_0 = 1$ THz device are shown in Figs. 3(a)-3(d). The electron concentration and electric field maps over the unit cell cross section are depicted in Figs. 3(a) and 3(b), where the unit cell mirror symmetry is exploited to show the maps corresponding to zero and maximum reverse bias ($V_{g,max} = -46$ V) in the left and right half of the unit cell, respectively. These results demonstrate a very efficient electrical switching effect, which is manifested through the voltage-dependent reflectance spectra in Fig. 3(c) (the numbers associated with curves denote $-V_g$) and the reflectance modulation RM > 90%. From the charge/discharge cycle in Fig. 3(d) and the calculated ps-order rise and fall times of the $Q(t)$ curve, we conclude that the proposed device has a very large intrinsic speed, which is a consequence of the deeply subwavelength separation of the driving electrodes.

Using the cavity geometry parameters that ensure critical coupling at full depletion from Fig. 2(a), we carry out a similar analysis for other $f_0$ values across the terahertz spectrum. The change of device geometry requires that the GaAs doping is adjusted as well, as shown in Fig. 3(e). The downscaling of cavity geometry required for operation at increasing frequencies, is seen to be accompanied by an approximately linear increase in the required doping (i.e. the maximum $N_d$ value which can be fully depleted), which in turn leads to a reduction of the $\omega_p/\omega_0$ ratio responsible for permittivity tuning according to Eq. (1). This causes the gradual decrease of the modulator performance RM shown in Fig. 3(f), as additionally evidenced from several representative modulator spectra shown in Fig. 3(g).

## 4. SUMMARY

The very high terahertz field confinement in arrays of metal-semiconductor-metal cavities with deeply subwavelength thickness may be combined with a reversely-biased Schottky junction in or close to the reach-through regime in order to provide a modulation performance on par or even exceeding best existing devices. Considering that the deep modulation and fast response of the latter require the use of elaborate structures, we believe that the simplification offered by employing the concepts discussed in this work will be of interest for the development of novel terahertz modulators.

## ACKNOWLEDGEMENTS

This work was funded by the Serbian Ministry of Education, Science and Technological Development under Grant ON171005 and by the Qatar National Research Fund (a member of the Qatar Foundation) through NPRP 8-028-1-001 and NPRP11S-1126-170033. G. Sinatkas and E.E. Kriezis are grateful for support by the Research Projects for Excellence IKY/Siemens. D.C. Zografopoulos and R. Beccherelli would also like to acknowledge support from COST Action CA 16220.

## REFERENCES

[1] R. Kersting *et al.*: Terahertz phase modulator, *Electron. Lett.*, vol. 36, no. 13, pp. 1156-1158, Jun. 2000.
[2] T. Kleine-Ostmann *et al.*: Room-temperature operation of an electrically driven terahertz modulator, *Appl. Phys. Lett.*, vol. 84, no. 18, pp. 3555-3557, 2004.
[3] R. Degl'Innocenti *et al.*: All-integrated terahertz modulators, *Nanophotonics*, vol. 7, pp. 127-144, 2018.
[4] H.-T. Chen *et al.*: Active terahertz metamaterial devices, *Nature*, vol. 444, pp. 597-600, 2006.

[5] H.-T. Chen *et al.*: A metamaterial solid-state terahertz phase modulator, *Nature Photon*., vol. 3, pp. 148-151, 2009.
[6] D. Shrekenhamer *et al*.: High speed terahertz modulation from metamaterials with embedded high electron mobility transistors, *Opt. Express*, vol. 19, no. 10, pp. 9968-9975, May 2011.
[7] N. Karl *et al*.: An electrically driven terahertz metamaterial diffractive modulator with more than 20 dB of dynamic range, *Appl. Phys. Lett*., vol. 104, no. 9, 2014, Art. no. 091115.
[8] Y. Zhang *et al*.: Gbps terahertz external modulator based on a composite metamaterial with a double-channel heterostructure, *Nano Lett*., vol. 15, no. 5, pp. 3501-3506, 2015.
[9] M.T. Nouman *et al*.: Terahertz modulator based on metamaterials integrated with metal-semiconductor-metal varactors, *Sci. Rep*., vol. 6, 2016, Art. no. 26452.
[10] Z. Zhou *et al*.: High performance metamaterials-high electron mobility transistors integrated terahertz modulator, *Opt. Express*, vol. 25, no. 15, pp. 17832-17840, Jul. 2017.
[11] M. Rahm *et al*.: THz wave modulators: A brief review on different modulation techniques, *J. Infrared Millimeter Terahertz Waves*, vol. 34, no. 1, pp. 1-27, 2013.
[12] B. Sensale-Rodriguez *et al.*: Extraordinary control of terahertz beam reflectance in graphene electro-absorption modulators, *Nano Lett*., vol. 12, no. 9, pp. 4518-4522, 2012.
[13] D. Shrekenhamer *et al*.: Liquid crystal tunable metamaterial absorber, *Phys. Rev. Lett*., vol. 110, Art. no. 177403, Apr. 2013.
[14] G. Isic *et al*.: Electrically tunable critically coupled terahertz metamaterial absorber based on nematic liquid crystals, *Phys. Rev. Appl.*, vol. 3, Art. no. 064007, Jun. 2015.
[15] B. Vasic *et al.*: Electrically tunable terahertz polarization converter based on overcoupled metal-isolator-metal metamaterials infiltrated with liquid crystals, *Nanotechnology*, vol. 28, no. 12, Art. no. 124002, 2017.
[16] G. Isic *et al*.: Electrically tunable metal-semiconductor-metal terahertz metasurface modulators, *IEEE J. Sel. Top. Quant*., vol. 25, no. 3, Art. no. 8500108, 2019.
[17] Y. Todorov *et al*.: Strong light-matter coupling in subwavelength metal-dielectric microcavities at terahertz frequencies, *Phys. Rev. Lett*., vol. 102, Art. no. 186402, May 2009.
[18] Y. Todorov *et al*.: Optical properties of metal-dielectric-metal microcavities in the THz frequency range, *Opt. Express*, vol. 18, no. 13, pp. 13886-13907, Jun. 2010.
[19] S. Fan *et al.*: Temporal coupled-mode theory for the Fano resonance in optical resonators, *J. Opt. Soc. Amer. A*, vol. 20, no. 3, pp. 569-572, Mar. 2003.
[20] G. Isic and R. Gajic: Geometrical scaling and modal decay rates in periodic arrays of deeply subwavelength terahertz resonators, *J. Appl. Phys*., vol. 116, no. 23, Art. no. 233103, 2014.
[21] G. Isic *et al.*: Plasmonic lifetimes and propagation lengths in metallodielectric superlattices, *Phys. Rev. B*, vol. 89, Art. no. 165427, Apr. 2014.
[22] C. Bulucea: Breakdown voltage of diffused epitaxial junctions, *Solid State Electron*., vol. 34, no. 12, pp. 1313-1318, 1991.
[23] G. Sinatkas *et al.*: Transparent conducting oxide electro-optic modulators on silicon platforms: A comprehensive study based on the drift-diffusion semiconductor model, *J. Appl. Phys.*, vol. 121, no. 2, Art. no. 023109, 2017.
[24] G. Sinatkas and E.E. Kriezis: Silicon-photonic electro-optic phase modulators integrating transparent conducting oxides, *IEEE J. Quantum. Electron*., vol. 54, no. 4, pp. 1-8, Aug. 2018.
[25] M. Sotoodeh *et al*.: Empirical low-field mobility model for III-V compounds applicable in device simulation codes, *J. Appl. Phys*., vol. 87, no. 6, pp. 2890-2900, 2000.
[26] D. Lockwood *et al*.: Optical phonon frequencies and damping in AlAs, GaP, GaAs, InP, InAs and InSb studied by oblique incidence infrared spectroscopy, *Solid State Commun*., vol. 136, no. 7, pp. 404-409, 2005.